Resolution-enhanced spectroscopy of ^{81}Y

H. Schnare, G. Winter,* L. Käubler, J. Reif, and R. Schwengner
Institut für Kern- und Hadronenphysik, Forschungszentrum Rossendorf, D-01314 Dresden, Germany

J. Döring,† G. D. Johns,‡ and S. L. Tabor
Physics Department, Florida State University, Tallahassee, Florida 32306

C. J. Gross
Oak Ridge Institute of Science and Education, Oak Ridge, Tennessee 37831

Y. A. Akovali, C. Baktash, and D. W. Stracener
Physics Division, Oak Ridge National Laboratory, Oak Ridge, Tennessee 37831

F. E. Durham
Department of Physics, Tulane University, New Orleans, Louisiana 70118

P. F. Hua, M. Korolija, D. R. LaFosse, and D. G. Sarantites
Chemistry Department, Washington University, St. Louis, Missouri 63130

I. Y. Lee, A. O. Macchiavelli, and W. Rathbun
Nuclear Science Division, Lawrence Berkeley National Laboratory, Berkeley, California 94720

A. Vander Molen
National Superconducting Cyclotron Laboratory, Michigan State University, East Lansing, Michigan 48824
(Received 26 March 1997)

The fusion-evaporation reaction ^{58}Ni(^{32}S,$2\alpha p$) has been used to study the neutron-deficient isotope ^{81}Y. Multiple particle γ-ray coincidences have been detected by the GAMMASPHERE array combined with the MICROBALL charged-particle detector system. Gamma-ray spectra with an improved resolution have been achieved from an event-by-event determination of the nucleus recoil momentum, thus allowing a precise Doppler-shift correction. In this way a resolution enhancement by a factor 2 was obtained for a 1 MeV γ line. During the analysis an E_γ-E_γ matrix as well as an E_γ-E_γ-E_γ cube have been used to extend the previously known level scheme to higher spin ($I \approx \frac{57}{2}$) and excitation energy ($E_x \approx 17$ MeV). More than 100 new γ rays and 80 new levels have been added to the level scheme and six new bands have been established. The interpretation of these bands in terms of the cranking model and their comparison with similar bands in neighboring nuclei is discussed. [S0556-2813(97)02908-7]

PACS number(s): 21.10.Re, 21.60.Cs, 23.20.Lv, 27.50.+e

I. INTRODUCTION

Nuclei in the mass region around $A=80$ have been found to exhibit a rich variety of structural behavior at high spins. Theoretical calculations [1,2] as well as experimental data have revealed properties like large deformation [3], shape coexistence [4], and superdeformation [5–10]. High-spin states in ^{81}Y ($N=Z+3$) were first established by Lister *et al.* [11]. Recently, in-beam γ-spectroscopy experiments with high-resolution γ detectors in conjunction with particle detectors have been performed by Mitarai *et al.* [12] and Johnson *et al.* [13]. Positive- and negative-parity rotational bands have been observed up to a tentative spin of $(\frac{45}{2}^+)$ and $(\frac{29}{2}^-)$ and levels up to an excitation energy of 11 MeV have been proposed.

Further investigation of the nuclear properties in such neutron-deficient nuclei is primarily hindered because of two experimental difficulties, resulting from (i) the large number of exit channels following the fusion-evaporation reaction implying a small relative cross section and an increased background from γ rays of neighboring nuclei, (ii) the large recoil velocity and its angular spread leading to a large Doppler broadening resulting in poor energy resolution in the observed γ-ray spectra.

In order to overcome the first difficulty, large γ-ray detector arrays with improved sensitivity have to be used. The second difficulty arises from a slowing down of the recoils in the target and from particle emission. Both effects contribute to the Doppler broadening and can be reduced by measuring the recoil angle and velocity with a highly segmented par-

*Deceased.

†Present address: Department of Physics, University of Notre Dame, Notre Dame, Indiana 46556.

‡Present address: Los Alamos National Laboratory, Los Alamos, New Mexico 87545.

ticle detector, thus allowing a precise Doppler-shift correction for γ rays emitted from the recoils.

The present paper presents the results of a measurement with the early implementation setup of the GAMMASPHERE array [14] and the MICROBALL 4π charged-particle detector array [15]. The high sensitivity of the GAMMASPHERE array as well as the selectivity of the MICROBALL have been essential to experimentally examine the level scheme of the nucleus ^{81}Y up to high excitation energies. On the basis of the recorded particle data a kinematic Doppler-shift correction was performed, resulting in a considerable improvement in the energy resolution of the observed γ lines.

II. EXPERIMENTAL DETAILS

High-spin states in the nucleus ^{81}Y were populated via the ^{58}Ni(^{32}S,$2\alpha p$) reaction. The 135 MeV ^{32}S beam was provided by the 88-inch Cyclotron of the Lawrence Berkeley National Laboratory and was focused on a self-supporting enriched ^{58}Ni target with an effective thickness of 283 μg/cm^2. Under these conditions the compound nucleus ^{90}Ru is formed with a maximum angular momentum of about $52\hbar$ according to fusion evaporation calculations. The main aim of the experiment was to study nuclei in the Zr region [6]. However, the nucleus ^{81}Y was weakly populated with respect to the total fusion cross section, $\sigma(^{81}\mathrm{Y}) \leq 1\%\ \sigma_{\mathrm{total}}$, but the highly sensitive detection method promised overwhelming new data.

Emitted γ rays from the target were detected with the early implementation phase of GAMMASPHERE, consisting of 36 Compton-suppressed Ge detectors. To reduce Doppler broadening, 30 detectors were placed in a forward-backward geometry with $\theta \leq 37°$ or $\geq 143°$, leaving the remaining six detectors at 90°. Evaporated light charged particles (p, d, t, and α) were detected with the 4π array MICROBALL, consisting of 95 CsI charged-particle detectors. Simultaneously this detector array permitted a clean separation between protons, deuterons, and α particles, and provided a precise angular information of the particle direction due to the high granularity. During the experiment only events which satisfied a γ-fold ≥ 3 condition in coincidence with particles detected by the MICROBALL were written to tape. Approximately 5.7×10^8 events were collected.

III. DATA ANALYSIS AND RESULTS

The recorded events were analyzed in several steps, each one focusing on a reduction of contaminating γ lines and the enhancement of energy resolution as well as a peak-to-background ratio in the observed γ-ray spectra.

In the first step, the charged particles from each event were identified as protons or alphas and from the analysis of different particle-γ coincidences the appropriate particle gate for the ^{81}Y exit channel was deduced. According to this selection the number of events was reduced to approximately 9×10^6, a fraction of approximately 1.6% of the total amount of data. This value is comparable to the expected relative cross section of the nucleus ^{81}Y in this reaction as predicted by fusion-evaporation calculations. Despite this small number of events a large gain in background reduction was achieved by requiring a coincidence with the selected charged particles. A comparison of the total projection and the particle-gated projection is shown in Fig. 1. Both projections are sums of spectra from individual detectors after correcting the average Doppler shift in each Ge detector with respect to the beam axis.

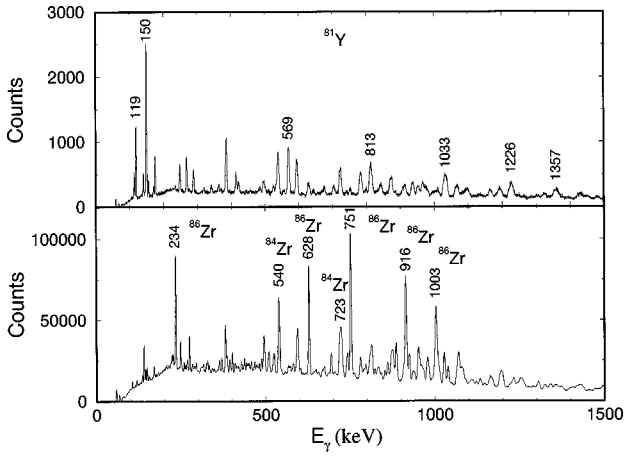

FIG. 1. Comparison of the total spectrum (bottom) and a particle-gated spectrum (top), representative for ^{81}Y. The particle gate required a coincidence with the $2\alpha1p$ exit channel.

A. Kinematic Doppler-shift correction

In order to investigate fast γ-ray transitions the experiment was performed with a thin target. In this way the observed γ rays were emitted from a ^{81}Y nucleus in flight, recoiling with a velocity of $v/c \approx 0.034$. Although the intrinsic energy resolution of a germanium detector is typically 2.5 keV for a 1 MeV γ line, the observed energy resolution in the ^{81}Y spectrum was about 12 keV after correcting for the Doppler shift in each detector with respect to the beam axis (conventional Doppler-shift correction). The bad resolution in the observed γ line is due to the opening angle of the germanium detector and the large cone angle of the residual nuclei by α and p emission in different directions, resulting in an increased Doppler broadening being observed in a fixed detector (see Fig. 2). In a conventional Doppler-shift correction, $\Delta E_\gamma^0 = \beta_0 E_\gamma \cos\vartheta_0$, the residual nucleus is assumed to recoil along the beam axis ($\beta_0 = v_0/c$) and recoil momenta of emitted particles are neglected. To enhance the resolution, the kinematic Doppler-shift correction method was applied to the data. From the MICROBALL data an event-by-event determination of the momenta of all emitted particles was

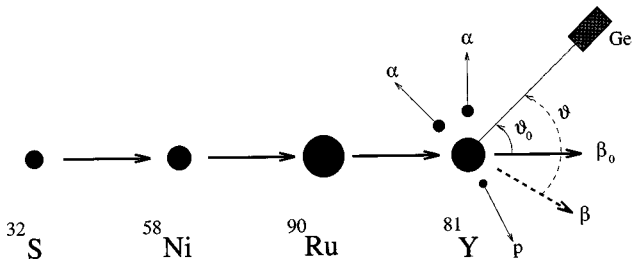

FIG. 2. Comparison between the conventional and kinematic Doppler-shift correction method. Angles and vectors are marked as described in the text.

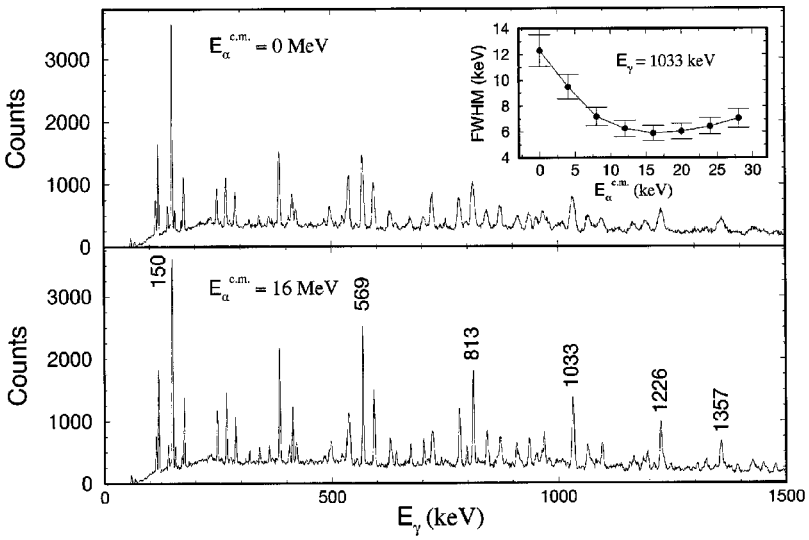

FIG. 3. Comparison of two total projections before (top) and after (bottom) kinematic Doppler-shift correction with different assumptions for the kinetic energy of the emitted α particle in the center-of-mass system ($E_\alpha^{\text{c.m.}}$). A kinetic energy of $E_\alpha^{\text{c.m.}}=0$ corresponds to the conventional Doppler-shift correction. The inset shows the obtained energy resolution for the 1033 keV γ line in the total projection as a function of the assumed $E_\alpha^{\text{c.m.}}$.

carried out and the nuclear recoil momentum was deduced on the basis of reaction kinematics. In this way improved values for the direction and the velocity of the recoiling nucleus were calculated. This allows a more precise Doppler-shift correction, $\Delta E_\gamma=\beta E_\gamma\cos\vartheta$, for each γ ray, detected at the angle ϑ with respect to the direction of the recoiling nucleus ($\beta=v/c$, Fig. 2).

Experimental difficulties resulted in unreliable energy calibrations for the particle detectors in the MICROBALL array. Therefore, assumptions about the kinetic energy of the emitted α and p had to be made. Proceeding on the fact that the kinetic energy of an evaporated α particle in the center-of-mass system $[E_{\text{kin}}^{\text{c.m.}}\simeq V_c(\text{MeV})\approx zZ/A^{1/3}]$ is approximately given by the Coulomb repulsion (V_c) between the emitted α particle (z) and the residual nucleus (Z,A), a value of 10–20 MeV is expected in the center-of-mass system.

To obtain an optimum average value, spectra with different assumptions for the kinetic energy of the α particle were sorted (Fig. 3). (The kinetic energy of the proton in the center-of-mass system was assumed to be $\frac{1}{2}\times E_\alpha$.) From each spectrum the FWHM of the 1033 keV γ line in ^{81}Y was deduced and plotted as a function of E_α (see inset in Fig. 3). The energy at the minimum of this curve, $E_\alpha=16$ MeV, was finally taken as the best guess for the kinetic energy of the α in the center-of-mass system. Because of the low curvature of this function close to the minimum, variations in the kinetic energy between 10 and 25 MeV only have a small influence on the width of the γ lines in the corrected spectra. The main effect in kinematic Doppler-shift correction turned out to be the directional correlation of all emitted particles and their influence on the initial momentum of the recoiling nucleus. During the sorting process the kinematic Doppler-shift correction was applied to the 9×10^6 high-fold events, belonging to ^{81}Y. These events were unpacked into 31×10^6 twofold coincidences as well as 13×10^6 threefold coincidences and sorted into an E_γ-E_γ matrix or an E_γ-E_γ-E_γ cube, respectively. Despite the low number of counts in the matrix and the cube, clean coincidence spectra could be produced due to the reduced background in the gate as the result of both the charged-particle gate and the enhanced resolution by kinematic Doppler-shift correction. The gain in E_γ resolution compared to the conventional Doppler-shift correction is shown in Fig. 4, e.g., the resolution of a 1 MeV γ line is improved by a factor of 2, to less than 6 keV. It should be noted that the improvement in energy resolution

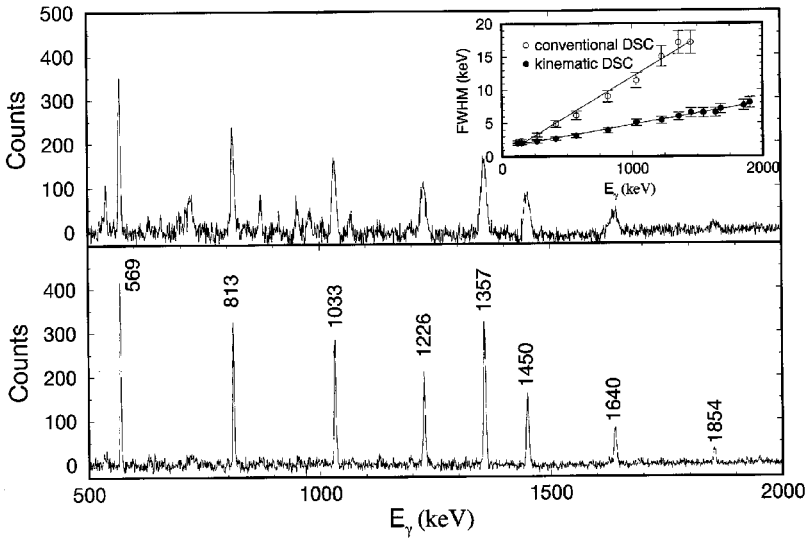

FIG. 4. Comparison of two coincidence spectra before (top) and after the kinematic Doppler-shift correction (bottom). Kinetic energies of $E_\alpha^{\text{c.m.}}=16$ MeV and $E_p^{\text{c.m.}}=8$ MeV were used for the emitted alpha and proton particles, respectively. The coincidence window was set on the $(\frac{41}{2}^+\rightarrow\frac{37}{2}^+)$ 1515 keV γ line. The inset shows the energy resolution of observed γ lines, as a function of E_γ for conventional and kinematic Doppler-shift correction (DSC).

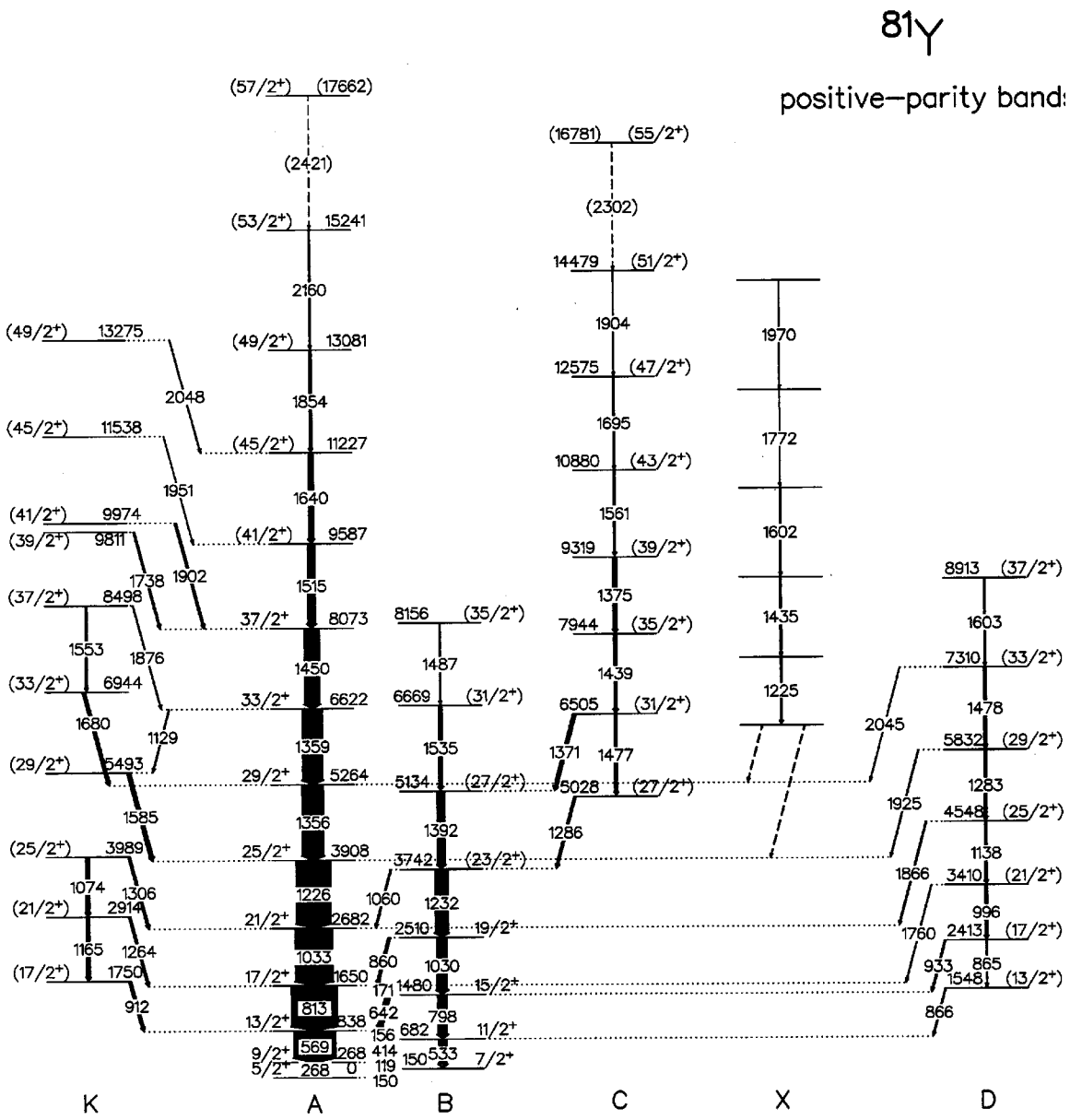

FIG. 5. Partial level scheme for the positive-parity bands of ^{81}Y, with energies in keV and uncertain spin and parity assignments in parentheses. The thickness of γ arrows reflects their intensity. Letters assigned to each band at the bottom of the figure indicate a name for the band, as referred in the text.

is accompanied by a simultaneous enhancement in the peak-to-background ratio in the observed γ spectra. Furthermore, spectra with less contaminating γ lines are produced as the consequence of a more precise placement of the coincidence window.

B. Coincidence analysis

Further analysis of the E_γ-E_γ coincidence matrix and the E_γ-E_γ-E_γ cube was performed with the Radware [16] software package. The combination of single-gated spectra from the twofold data and the double-gated spectra from the cube provided the sensitivity required for the study of high-spin bands and their linking transitions to the low-lying states of the nucleus. The analysis method of the kinematic Doppler-shift correction and the use of double-gated spectra extracted from the cube proved to be essential for the determination of the complex level scheme of ^{81}Y. The level scheme was built on the basis of coincidence relations and relative intensities as well as γ-ray energy sums.

Information on the transition multipolarities was obtained by using the method of directional correlation from oriented states (DCO). For this purpose the $\gamma\gamma$ coincidences were stored in a matrix with axes representing the energies of γ rays emitted from detectors in forward-backward geometry ($\theta \leqslant 37°$ or $\geqslant 143°$) against detectors at $\theta = 90°$. Due to the small number of counts in the DCO matrix ($\approx 3.5\times10^6$) unambiguous multipole orders were only obtained for the lowest γ-ray transitions in the positive-parity yrast band. Therefore spin-parity assignments of the higher energy levels are based on known systematic structures in neighboring nu-

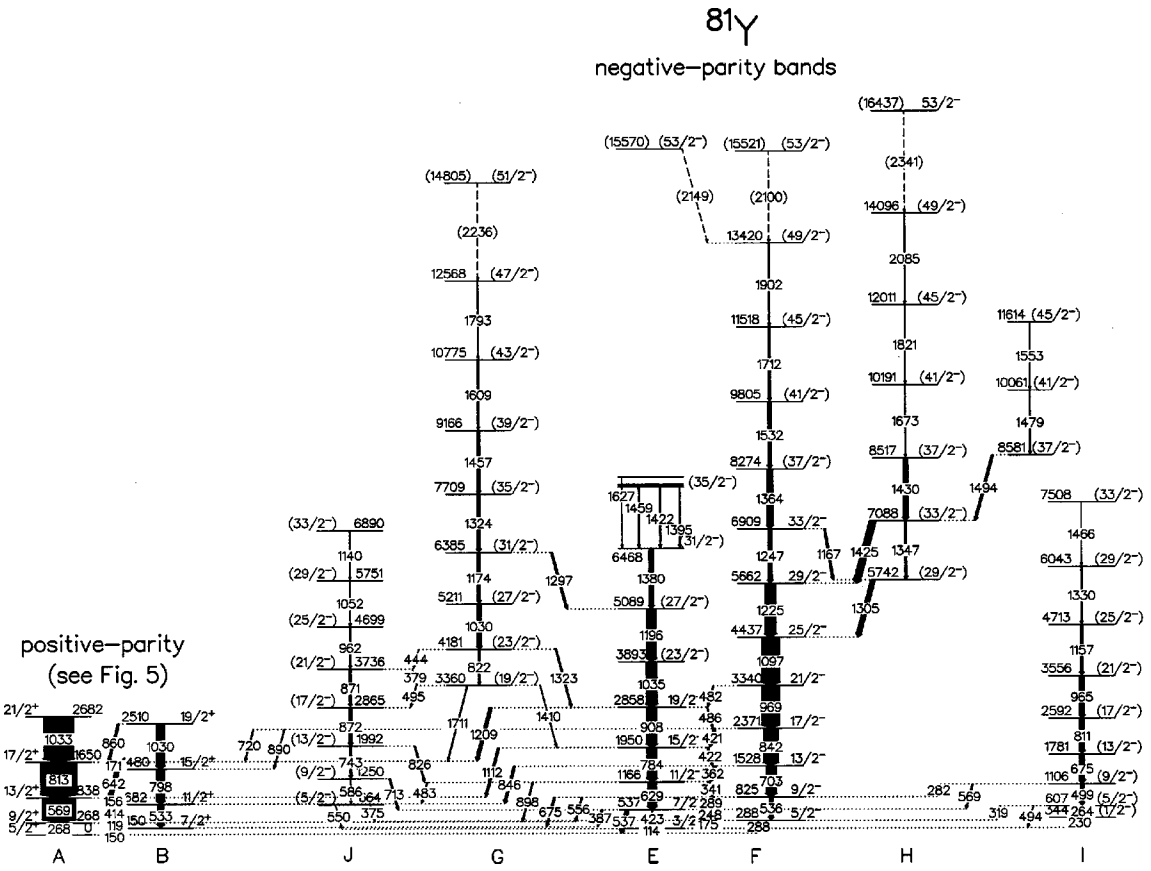

FIG. 6. Partial level scheme for the negative-parity bands of ^{81}Y (see also previous figure).

clei and earlier measurements of this nucleus [12,13].

IV. LEVEL SCHEME OF ^{81}Y

The level scheme of ^{81}Y, based on the present work, is presented in Figs. 5 and 6, with the widths of the transitions proportional to the measured intensities. Any tentative spin-parity assignments in the level scheme not resulting from DCO ratios have been put into parentheses. Compared to the level scheme of ^{81}Y obtained from earlier experiments, the present study with GAMMASPHERE and MICROBALL has made a substantial improvement in the γ-ray spectra at high energies leading to an extension of spectroscopic information in this nucleus to higher spins, including six new bands. Table I summarizes the deduced levels, γ energies, proposed spins, and parities.

A. Positive-parity bands, A and B

In the previously reported level scheme of ^{81}Y [12,13], the favored signature of the yrast band **A** with $(\pi,\alpha)=(+,+\frac{1}{2})$, was observed up to a spin $I^{\pi}=(\frac{45}{2}^{+})$. In the present study that placement of levels was confirmed up to $I^{\pi}=\frac{29}{2}^{+}$, whereas some discrepancies were observed concerning the extension of the band. The 1365 keV transition proposed by Mitarai *et al.* [12] and Johnson *et al.* [13] to populate the $I^{\pi}=\frac{29}{2}^{+}$ level was corrected downwards in energy to 1359 keV, extended by a sequence of γ lines with 1450, 1515, 1640, 1854, 2160, and tentatively 2421 keV at an excitation energy of $E_x=17.7$ MeV. The γ lines up to the 1854 keV transition are clearly seen in the single-gated spectrum of Fig. 4, which was already discussed in connection with the resolution enhancement. Here a single gate was placed on the 1515 keV transition deexciting the $I^{\pi}=(\frac{41}{2}^{+})$ state. Note the higher relative intensity in the 1357 keV γ line, resulting from the 1356/1359 keV γ-ray sequence. This sequence of γ lines was further confirmed with different combinations of double-gated spectra deduced from the cube. Figure 7 shows at the bottom a spectrum of the $(+,+\frac{1}{2})$ yrast band, labeled **A**, created by combining all possible double gates on the six γ-ray transitions between 1359 and 2160 keV of this band.

In addition, several γ-ray transitions (e.g., 912, 1264, 1306 keV, . . .) originating from levels placed as sequence **K** in Fig. 5 were observed to feed different levels of the $(+,+\frac{1}{2})$ yrast band **A**. The coincidence spectra gated on these lines did not reveal any more evidence of other coincident γ lines as those shown in Fig. 5 and no extended band structures in connection with the observed transitions have been established. A similar feature was also reported in the yrast band of the neighboring odd nucleus ^{83}Y [17].

In the unfavored $(+,-\frac{1}{2})$ yrast band **B** the previously reported 934 keV transition, assigned to populate the $I^{\pi}=\frac{15}{2}^{+}$ level, was not confirmed as a band member. Instead a continuation of this band by 1030, 1232, 1392, 1535, and 1487 keV γ lines is proposed. These placements are supported by the observation of several new interband transitions connecting both signatures of the positive-parity yrast

TABLE I. Levels and transition energies in ^{81}Y.

E_i (keV)	E_f (keV)	E_γ (keV)[a]	I_i^π [b]	I_f^π [b]	Band$_i$ [c]	Band$_f$ [c]
Positive parity						
149.7	0.0	149.7	$\frac{7}{2}^+$	$\frac{5}{2}^+$	*B*	*A*
268.4	149.7	119.2	$\frac{9}{2}^+$	$\frac{7}{2}^+$	*A*	*B*
	0.0	268.4	$\frac{9}{2}^+$	$\frac{5}{2}^+$	*A*	*A*
682.3	268.4	414.0	$\frac{11}{2}^+$	$\frac{9}{2}^+$	*B*	*A*
	149.7	532.6	$\frac{11}{2}^+$	$\frac{7}{2}^+$	*B*	*B*
837.6	682.3	155.7	$\frac{13}{2}^+$	$\frac{11}{2}^+$	*A*	*B*
	268.4	569.3	$\frac{13}{2}^+$	$\frac{9}{2}^+$	*A*	*A*
1480.2	837.6	642.5	$\frac{15}{2}^+$	$\frac{13}{2}^+$	*B*	*A*
	682.3	798.2	$\frac{15}{2}^+$	$\frac{11}{2}^+$	*B*	*B*
1548.5	682.3	866.2	$(\frac{13}{2}^+)$	$\frac{11}{2}^+$	*D*	*B*
1649.9	1480.2	170.5	$\frac{17}{2}^+$	$\frac{15}{2}^+$	*A*	*B*
	837.6	813.1	$\frac{17}{2}^+$	$\frac{13}{2}^+$	*A*	*A*
1749.5	837.6	911.8	$(\frac{17}{2}^+)$	$\frac{13}{2}^+$	*K*	*A*
2413.4	1548.5	864.9	$(\frac{17}{2}^+)$	$(\frac{13}{2}^+)$	*D*	*D*
	1480.2	932.7	$(\frac{17}{2}^+)$	$\frac{15}{2}^+$	*D*	*B*
2510.1	1649.9	859.9	$\frac{19}{2}^+$	$\frac{17}{2}^+$	*B*	*A*
	1480.2	1030.3	$\frac{19}{2}^+$	$\frac{15}{2}^+$	*B*	*B*
2682.4	1649.9	1032.8	$\frac{21}{2}^+$	$\frac{17}{2}^+$	*A*	*A*
2914.4	1749.5	1164.7	$(\frac{21}{2}^+)$	$(\frac{17}{2}^+)$	*K*	*K*
	1649.9	1264.5	$(\frac{21}{2}^+)$	$\frac{17}{2}^+$	*K*	*A*
3410.1	2413.4	996.2	$(\frac{21}{2}^+)$	$(\frac{17}{2}^+)$	*D*	*D*
	1649.9	1760.5	$(\frac{21}{2}^+)$	$\frac{17}{2}^+$	*D*	*A*
3742.1	2682.4	1059.6	$(\frac{23}{2}^+)$	$\frac{21}{2}^+$	*B*	*A*
	2510.1	1232.1	$(\frac{23}{2}^+)$	$\frac{19}{2}^+$	*B*	*B*
3907.8	2682.4	1226.0	$\frac{25}{2}^+$	$\frac{21}{2}^+$	*A*	*A*
3988.6	2914.4	1074.1	$(\frac{25}{2}^+)$	$(\frac{21}{2}^+)$	*K*	*K*
	2682.4	1306.3	$(\frac{25}{2}^+)$	$\frac{21}{2}^+$	*K*	*A*
4548.3	3410.1	1137.8	$(\frac{25}{2}^+)$	$(\frac{21}{2}^+)$	*D*	*D*
	2682.4	1865.5	$(\frac{25}{2}^+)$	$\frac{21}{2}^+$	*D*	*A*
5028.3	3742.1	1286.0	$(\frac{27}{2}^+)$	$(\frac{23}{2}^+)$	*C*	*B*
5134.2	3742.1	1392.3	$(\frac{27}{2}^+)$	$(\frac{23}{2}^+)$	*B*	*B*
5263.7	3907.8	1356.0	$\frac{29}{2}^+$	$\frac{25}{2}^+$	*A*	*A*
5493.0	3907.8	1585.1	$(\frac{29}{2}^+)$	$\frac{25}{2}^+$	*K*	*A*
5831.8	4548.3	1282.8	$(\frac{29}{2}^+)$	$(\frac{25}{2}^+)$	*D*	*D*
	3907.8	1925.1	$(\frac{29}{2}^+)$	$\frac{25}{2}^+$	*D*	*A*
6505.3	5134.2	1371.3	$(\frac{31}{2}^+)$	$(\frac{27}{2}^+)$	*C*	*B*
	5028.3	1476.8	$(\frac{31}{2}^+)$	$(\frac{27}{2}^+)$	*C*	*C*
6622.3	5493.0	1129.2	$(\frac{33}{2}^+)$	$(\frac{29}{2}^+)$	*A*	*K*
	5263.7	1359.0	$(\frac{33}{2}^+)$	$\frac{29}{2}^+$	*A*	*A*
6668.9	5134.2	1534.7	$(\frac{31}{2}^+)$	$(\frac{27}{2}^+)$	*B*	*B*
6943.9	5263.7	1679.9	$(\frac{33}{2}^+)$	$\frac{29}{2}^+$	*K*	*A*
7310.2	5831.8	1478.4	$(\frac{33}{2}^+)$	$\frac{29}{2}^+$	*D*	*D*
	5263.7	2045.1	$(\frac{33}{2}^+)$	$\frac{29}{2}^+$	*D*	*A*
7943.9	6505.3	1438.6	$(\frac{35}{2}^+)$	$(\frac{31}{2}^+)$	*C*	*C*
8072.7	6622.3	1450.4	$(\frac{37}{2}^+)$	$(\frac{33}{2}^+)$	*A*	*A*
8156.3	6668.9	1487.4	$(\frac{35}{2}^+)$	$(\frac{31}{2}^+)$	*B*	*B*
8497.7	6943.9	1553.5	$(\frac{37}{2}^+)$	$(\frac{33}{2}^+)$	*K*	*K*

TABLE I. (*Continued*).

E_i (keV)	E_f (keV)	E_γ (keV)[a]	I_i^π [b]	I_f^π [b]	Band$_i$ [c]	Band$_f$ [c]
	6622.3	1875.8	$(\frac{37}{2}^+)$	$(\frac{33}{2}^+)$	*K*	*A*
8912.8	7310.2	1602.5	$(\frac{37}{2}^+)$	$(\frac{33}{2}^+)$	*D*	*D*
9318.7	7943.9	1374.8	$(\frac{39}{2}^+)$	$(\frac{35}{2}^+)$	*C*	*C*
9587.3	8072.7	1514.6	$(\frac{41}{2}^+)$	$(\frac{37}{2}^+)$	*A*	*A*
9810.9	8072.7	1738.2	$(\frac{39}{2}^+)$	$(\frac{37}{2}^+)$	*K*	*A*
9974.3	8072.7	1901.6	$(\frac{41}{2}^+)$	$(\frac{37}{2}^+)$	*K*	*A*
10879.8	9318.7	1561.2	$(\frac{43}{2}^+)$	$(\frac{39}{2}^+)$	*C*	*C*
11226.9	9587.3	1639.6	$(\frac{45}{2}^+)$	$(\frac{41}{2}^+)$	*A*	*A*
11538.1	9587.3	1950.9	$(\frac{45}{2}^+)$	$(\frac{41}{2}^+)$	*K*	*A*
12575.2	10879.8	1695.3	$(\frac{47}{2}^+)$	$(\frac{43}{2}^+)$	*C*	*C*
13080.9	11226.9	1854.0	$(\frac{49}{2}^+)$	$(\frac{45}{2}^+)$	*A*	*A*
13275.0	11226.9	2048.1	$(\frac{49}{2}^+)$	$(\frac{45}{2}^+)$	*K*	*A*
14478.7	12575.2	1904.1	$(\frac{51}{2}^+)$	$(\frac{47}{2}^+)$	*C*	*C*
15240.5	13080.9	2160.2	$(\frac{53}{2}^+)$	$(\frac{49}{2}^+)$	*A*	*A*
16780.5	14478.7	(2301.8)	$(\frac{55}{2}^+)$	$(\frac{51}{2}^+)$	*C*	*C*
17661.9	15240.5	(2421.3)	$(\frac{57}{2}^+)$	$(\frac{53}{2}^+)$	*A*	*A*
		1225.0			*X*	*X*
		1434.6			*X*	*X*
		1601.9			*X*	*X*
		1772.3			*X*	*X*
		1969.9			*X*	*X*
Negative parity						
113.4	0.0	113.4	$\frac{3}{2}^-$	$\frac{5}{2}^+$	*E*	*A*
288.4	113.4	175.3	$\frac{5}{2}^-$	$\frac{3}{2}^-$	*F*	*E*
	0.0	288.4	$\frac{5}{2}^-$	$\frac{5}{2}^+$	*F*	*A*
343.5	113.4	230.1	$(\frac{1}{2}^-)$	$\frac{3}{2}^-$	*I*	*E*
536.5	288.4	248.3	$\frac{7}{2}^-$	$\frac{5}{2}^-$	*E*	*F*
	149.7	386.5	$\frac{7}{2}^-$	$\frac{7}{2}^+$	*E*	*B*
	113.4	423.2	$\frac{7}{2}^-$	$\frac{3}{2}^-$	*E*	*E*
	0.0	536.5	$\frac{7}{2}^-$	$\frac{5}{2}^+$	*E*	*A*
607.4	343.5	264.0	$(\frac{5}{2}^-)$	$(\frac{1}{2}^-)$	*I*	*I*
	288.4	319.0	$(\frac{5}{2}^-)$	$\frac{5}{2}^-$	*I*	*F*
	113.4	493.8	$(\frac{5}{2}^-)$	$\frac{3}{2}^-$	*I*	*E*
663.5	288.4	375.0	$(\frac{5}{2}^-)$	$\frac{5}{2}^-$	*J*	*F*
	113.4	549.9	$(\frac{5}{2}^-)$	$\frac{3}{2}^-$	*J*	*E*
824.8	536.5	288.6	$\frac{9}{2}^-$	$\frac{7}{2}^-$	*F*	*E*
	288.4	536.3	$\frac{9}{2}^-$	$\frac{5}{2}^-$	*F*	*F*
	268.4	556.0	$\frac{9}{2}^-$	$\frac{9}{2}^+$	*F*	*A*
	149.7	674.9	$\frac{9}{2}^-$	$\frac{7}{2}^+$	*F*	*B*
1106.2	824.8	281.8	$(\frac{9}{2}^-)$	$\frac{9}{2}^-$	*I*	*F*
	607.4	498.9	$(\frac{9}{2}^-)$	$(\frac{5}{2}^-)$	*I*	*I*
	536.5	569.4	$(\frac{9}{2}^-)$	$\frac{7}{2}^-$	*I*	*E*
1165.8	824.8	340.8	$\frac{11}{2}^-$	$\frac{9}{2}^-$	*E*	*F*
	682.3	483.1	$\frac{11}{2}^-$	$\frac{11}{2}^+$	*E*	*B*
	536.5	629.1	$\frac{11}{2}^-$	$\frac{7}{2}^-$	*E*	*E*
	268.4	897.8	$\frac{11}{2}^-$	$\frac{9}{2}^+$	*E*	*A*
1249.6	663.5	585.8	$(\frac{9}{2}^-)$	$(\frac{5}{2}^-)$	*J*	*J*

TABLE I. (*Continued*).

E_i (keV)	E_f (keV)	E_γ (keV)[a]	I_i^π [b]	I_f^π [b]	Band$_i$ [c]	Band$_f$ [c]
	536.5	713.0	$(\frac{9}{2}^-)$	$\frac{7}{2}^-$	*J*	*E*
1528.1	1165.8	362.3	$\frac{13}{2}^-$	$\frac{11}{2}^-$	*F*	*E*
	824.8	703.1	$\frac{13}{2}^-$	$\frac{9}{2}^-$	*F*	*F*
	682.3	845.8	$\frac{13}{2}^-$	$\frac{11}{2}^+$	*F*	*B*
1780.7	1106.2	674.5	$(\frac{13}{2}^-)$	$(\frac{9}{2}^-)$	*I*	*I*
1949.9	1528.1	421.9	$\frac{15}{2}^-$	$\frac{13}{2}^-$	*E*	*F*
	1165.8	783.8	$\frac{15}{2}^-$	$\frac{11}{2}^-$	*E*	*E*
	837.6	1112.3	$\frac{15}{2}^-$	$\frac{13}{2}^+$	*E*	*A*
1992.3	1249.6	742.5	$(\frac{13}{2}^-)$	$(\frac{9}{2}^-)$	*J*	*J*
	1165.8	826.3	$(\frac{13}{2}^-)$	$\frac{11}{2}^-$	*J*	*E*
2370.7	1949.9	421.1	$\frac{17}{2}^-$	$\frac{15}{2}^-$	*F*	*E*
	1649.9	720.2	$\frac{17}{2}^-$	$\frac{17}{2}^+$	*F*	*A*
	1528.1	842.4	$\frac{17}{2}^-$	$\frac{13}{2}^-$	*F*	*F*
	1480.2	890.1	$\frac{17}{2}^-$	$\frac{15}{2}^+$	*F*	*B*
2591.8	1780.7	811.1	$(\frac{17}{2}^-)$	$(\frac{13}{2}^-)$	*I*	*I*
2858.1	2370.7	486.3	$\frac{19}{2}^-$	$\frac{17}{2}^-$	*E*	*F*
	1949.9	907.9	$\frac{19}{2}^-$	$\frac{15}{2}^-$	*E*	*E*
	1649.9	1208.7	$\frac{19}{2}^-$	$\frac{17}{2}^+$	*E*	*A*
2864.9	1992.3	872.2	$(\frac{17}{2}^-)$	$(\frac{13}{2}^-)$	*J*	*J*
3340.0	2858.1	481.9	$\frac{21}{2}^-$	$\frac{19}{2}^-$	*F*	*E*
	2370.7	969.2	$\frac{21}{2}^-$	$\frac{17}{2}^-$	*F*	*F*
3359.6	2864.9	494.6	$(\frac{19}{2}^-)$	$(\frac{17}{2}^-)$	*G*	*J*
	1949.9	1409.7	$(\frac{19}{2}^-)$	$\frac{15}{2}^-$	*G*	*E*
	1649.9	1709.7	$(\frac{19}{2}^-)$	$\frac{17}{2}^+$	*G*	*A*
3556.4	2591.8	964.6	$(\frac{21}{2}^-)$	$(\frac{17}{2}^-)$	*I*	*I*
3736.2	3359.6	378.7	$(\frac{21}{2}^-)$	$(\frac{19}{2}^-)$	*J*	*G*
	2864.9	870.9	$(\frac{21}{2}^-)$	$(\frac{17}{2}^-)$	*J*	*J*
3893.0	2858.1	1035.2	$(\frac{23}{2}^-)$	$\frac{19}{2}^-$	*E*	*E*
4180.7	3736.2	444.1	$(\frac{23}{2}^-)$	$(\frac{21}{2}^-)$	*G*	*J*
	3359.6	821.9	$(\frac{23}{2}^-)$	$(\frac{19}{2}^-)$	*G*	*G*
	2858.1	1322.6	$(\frac{23}{2}^-)$	$\frac{19}{2}^-$	*G*	*E*
4437.0	3340.0	1097.0	$(\frac{25}{2}^-)$	$\frac{21}{2}^-$	*F*	*F*
4698.6	3736.2	962.3	$(\frac{25}{2}^-)$	$(\frac{21}{2}^-)$	*J*	*J*
4713.3	3556.4	1156.9	$(\frac{25}{2}^-)$	$(\frac{21}{2}^-)$	*I*	*I*
5088.6	3893.0	1195.9	$(\frac{27}{2}^-)$	$(\frac{23}{2}^-)$	*E*	*E*
5210.9	4180.7	1029.9	$(\frac{27}{2}^-)$	$(\frac{23}{2}^-)$	*G*	*G*
5662.1	4437.0	1224.8	$(\frac{29}{2}^-)$	$(\frac{25}{2}^-)$	*F*	*F*
5741.7	4437.0	1305.1	$(\frac{29}{2}^-)$	$(\frac{25}{2}^-)$	*H*	*F*
5750.5	4698.6	1052.0	$(\frac{29}{2}^-)$	$(\frac{25}{2}^-)$	*J*	*J*
6042.8	4713.3	1329.5	$(\frac{29}{2}^-)$	$(\frac{25}{2}^-)$	*I*	*I*
6384.9	5210.9	1173.6	$(\frac{31}{2}^-)$	$(\frac{27}{2}^-)$	*G*	*G*
	5088.6	1296.7	$(\frac{31}{2}^-)$	$(\frac{27}{2}^-)$	*G*	*E*
6468.5	5088.6	1379.9	$(\frac{31}{2}^-)$	$(\frac{27}{2}^-)$	*E*	*E*
6890.3	5750.5	1139.8	$(\frac{33}{2}^-)$	$(\frac{29}{2}^-)$	*J*	*J*
6909.2	5741.7	1167.0	$(\frac{33}{2}^-)$	$(\frac{29}{2}^-)$	*F*	*H*
	5662.1	1247.4	$(\frac{33}{2}^-)$	$(\frac{29}{2}^-)$	*F*	*F*
7087.7	5741.7	1346.7	$(\frac{33}{2}^-)$	$(\frac{29}{2}^-)$	*H*	*H*

TABLE I. (*Continued*).

E_i (keV)	E_f (keV)	E_γ (keV)[a]	I_i^π [b]	I_f^π [b]	Band$_i$ [c]	Band$_f$ [c]
	5662.1	1424.9	$(\frac{33}{2}^-)$	$(\frac{29}{2}^-)$	*H*	*F*
7508.4	6042.8	1465.6	$(\frac{33}{2}^-)$	$(\frac{29}{2}^-)$	*I*	*I*
7709.0	6384.9	1324.1	$(\frac{35}{2}^-)$	$(\frac{31}{2}^-)$	*G*	*G*
7863.0	6468.5	1394.5	$(\frac{35}{2}^-)$	$(\frac{31}{2}^-)$	*E*	*E*
7890.9	6468.5	1422.4	$(\frac{35}{2}^-)$	$(\frac{31}{2}^-)$	*E*	*E*
7927.2	6468.5	1458.7	$(\frac{35}{2}^-)$	$(\frac{31}{2}^-)$	*E*	*E*
8095.5	6468.5	1627.0	$(\frac{35}{2}^-)$	$(\frac{31}{2}^-)$	*E*	*E*
8273.6	6909.2	1364.4	$(\frac{37}{2}^-)$	$(\frac{33}{2}^-)$	*F*	*F*
8517.3	7087.7	1429.5	$(\frac{37}{2}^-)$	$(\frac{33}{2}^-)$	*H*	*H*
8581.3	7087.7	1493.6	$(\frac{37}{2}^-)$	$(\frac{33}{2}^-)$	*I*	*H*
9165.9	7709.0	1456.9	$(\frac{39}{2}^-)$	$(\frac{35}{2}^-)$	*G*	*G*
9805.5	8273.6	1531.9	$(\frac{41}{2}^-)$	$(\frac{37}{2}^-)$	*F*	*F*
10060.8	8581.3	1479.5	$(\frac{41}{2}^-)$	$(\frac{37}{2}^-)$	*I*	*I*
10190.6	8517.3	1673.3	$(\frac{41}{2}^-)$	$(\frac{37}{2}^-)$	*H*	*H*
10775.4	9165.9	1609.5	$(\frac{43}{2}^-)$	$(\frac{39}{2}^-)$	*G*	*G*
11517.9	9805.5	1712.4	$(\frac{45}{2}^-)$	$(\frac{41}{2}^-)$	*F*	*F*
11613.9	10060.8	1553.1	$(\frac{45}{2}^-)$	$(\frac{41}{2}^-)$	*I*	*I*
12011.3	10190.6	1820.7	$(\frac{45}{2}^-)$	$(\frac{41}{2}^-)$	*H*	*H*
12568.3	10775.4	1792.9	$(\frac{47}{2}^-)$	$(\frac{43}{2}^-)$	*G*	*G*
13420.3	11517.9	1902.5	$(\frac{49}{2}^-)$	$(\frac{45}{2}^-)$	*F*	*F*
14096.1	12011.3	2085.4	$(\frac{49}{2}^-)$	$(\frac{45}{2}^-)$	*H*	*H*
14805.0	12568.3	(2235.5)	$(\frac{51}{2}^-)$	$(\frac{47}{2}^-)$	*G*	*G*
15520.5	13420.3	(2100.2)	$(\frac{53}{2}^-)$	$(\frac{49}{2}^-)$	*F*	*F*
15570.5	13420.3	(2149.2)	$(\frac{53}{2}^-)$	$(\frac{49}{2}^-)$	*E*	*F*
16437.2	14096.1	(2340.9)	$(\frac{53}{2}^-)$	$(\frac{49}{2}^-)$	*H*	*H*

[a]Typical error in E_γ is 0.1%.

[b]Typical error for uncertain spin assignments (in parentheses) is $1\hbar$.

[c]Indicates the assignment of levels to the bands as shown in the level scheme (Figs. 5 and 6).

band, especially the 860 keV $(\frac{19}{2}^+ \rightarrow \frac{17}{2}^+)$ and 1060 keV $[(\frac{23}{2}^+) \rightarrow \frac{21}{2}^+]$ transitions feeding the $(+,+\frac{1}{2})$ band. These assignments are illustrated in spectrum **B** of Fig. 7, deduced from a sum of double-gated spectra.

B. Negative-parity bands, E, F, and I

The $(-,-\frac{1}{2})$ band **E** was extended by two more transitions up to a spin of $(\frac{31}{2}^-)$ and an excitation energy of $E_x = 6.5$ MeV. Several parallel transitions with 1395, 1422, 1459, and 1627 keV were observed to populate the $(\frac{31}{2}^-)$ level, but the weak intensity in each individual branch limits further identification with respect to the continuation of the band.

The $(-,+\frac{1}{2})$ band **F** was extended by five new transitions with 1247, 1364, 1532, 1712, and 1902 keV up to a spin of $(\frac{49}{2}^-)$ and an excitation energy of $E_x = 13.4$ MeV. Two parallel transitions with 2100 and 2149 keV were tentatively identified to feed the highest level of this band. Remarkable is the forking of the band above the $(\frac{25}{2}^-)$ level, which was deduced from a detailed analysis of relative intensities and coincidence relations of involved γ lines. This forking is built up by two decay branches depopulating the $(\frac{33}{2}^-)$ level, via a 1247/1225 keV and a 1167/1305 keV sequence. In this way two $(\frac{29}{2}^-)$ levels were found with a separation of 80 keV. In the progress of analysis, one of those levels was discovered to belong to a new band, named **H**. Furthermore, the sequence of $\Delta I = 1$ interband transitions between bands **E** and **F** was extended by a 482 keV transition feeding the $\frac{19}{2}^-$ level of the $(-,-\frac{1}{2})$ band **E** and a 486 keV transition populating the $\frac{17}{2}^-$ level of the $(-,+\frac{1}{2})$ band **F**. In addition several $E1$ transitions were observed connecting the negative-parity states with the positive-parity states.

A third sequence of γ lines, belonging to the band labeled **I** in the level scheme, was already reported by Mitarai *et al.* [12] and confirmed later by Johnson *et al.* [13]. Three more transitions with 1157, 1330, and 1466 keV were added to this band up to an excitation energy of 7.5 MeV and several transitions decaying out of the band at the bottom, were identified. Furthermore, low-energy γ rays with 230 and 264 keV

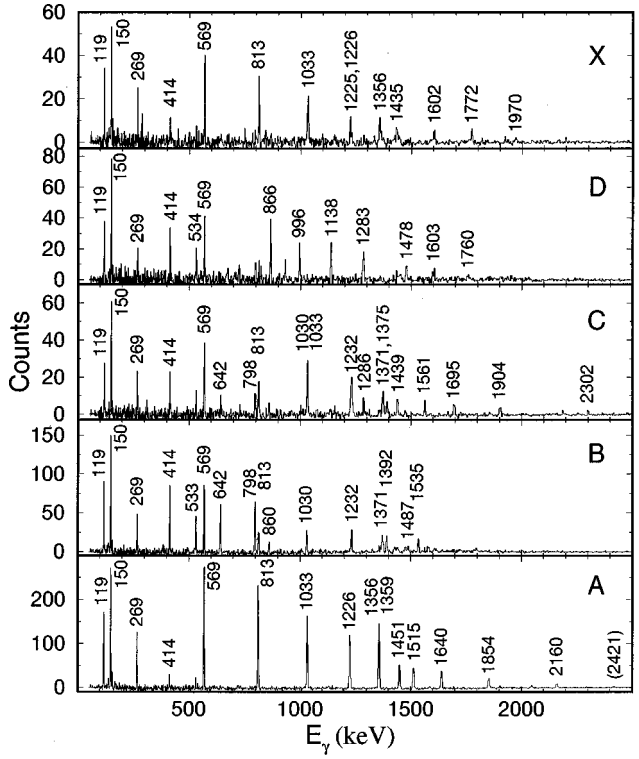

FIG. 7. Typical γ-ray spectra for the positive-parity bands. The spectra were created by summing double-gated spectra from the E_γ-E_γ-E_γ cube data.

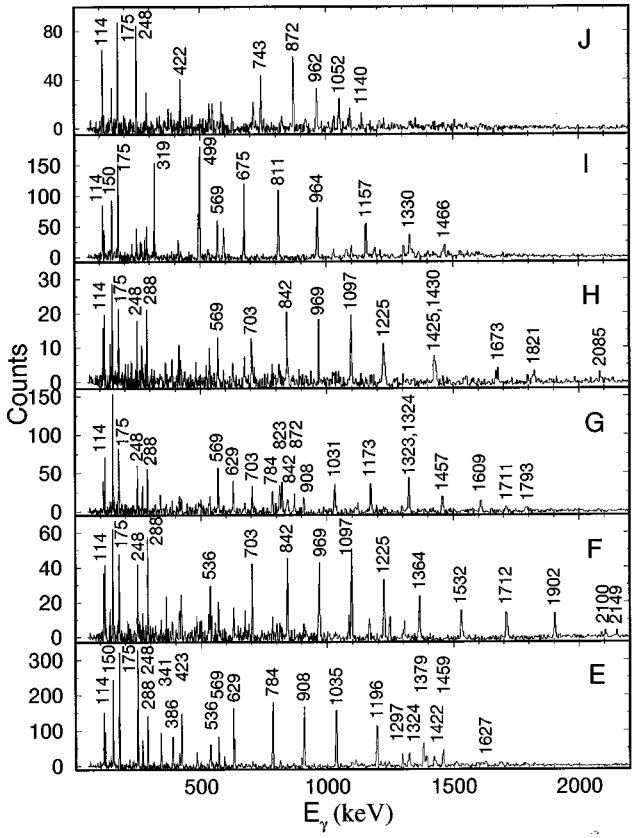

FIG. 8. Typical γ-ray spectra for the negative-parity bands. The spectra were created by summing double-gated spectra from the E_γ-E_γ-E_γ cube data.

were observed to be in coincidence with all band members except the 494 keV transition, feeding the $\frac{3}{2}^-$ level. This observation suggests the placement of a new level at 344 keV or 377 keV. We propose the 344 keV level as the $\frac{1}{2}^-$ bandhead of band **I**, since no further γ lines have been observed to populate the new level. The regular sequence of γ transitions in band **I** support a collective rotational interpretation for this band. A weak intensity of the band and the levels populated by γ lines decaying out of the band suggest the indicated spin values as the most probable one. Representative spectra for the bands **E**, **F**, and **I** are illustrated in Fig. 8.

C. New bands, C, D, G, H, J, and X

In addition, six new rotational bands, labeled **C**, **D**, **G**, **H**, **J**, and **X**, were extracted from the data. Typical double-gated coincidence spectra for these bands are presented in Figs. 7 and 8. The regular energy spacing of the γ rays in these bands provides strong evidence for their rotational character. As shown in the level scheme (Figs. 5 and 6) the bands, **C**, **D**, and **X**, are probably of positive parity, whereas the bands **G**, **H**, and **J** have possibly negative parity.

In band **C** a cascade of six γ lines, plus tentatively a 2302 keV transition at the top of the band, were observed and two γ-ray transitions (1286, 1371 keV) deexciting this band into the $(\frac{23}{2}^+)$ and $(\frac{27}{2}^+)$ level of band **B** were identified. Due to this decay, the levels in band **C** have, compared to the levels in band **B** with the same spin, a lower excitation energy, favoring the population of band **C** above spin $I \approx (\frac{27}{2}^+)$. Hence, band **C** is becoming yrast with respect to band **B**.

Six γ-ray transitions were found for band **D** and their placement is clearly supported by the observation of several γ-ray connections to the positive-parity yrast bands **A** and **B**. At high spins the deexcitation out of this band favors yrast levels with positive signature (band **A**) whereas at low spins the opposite was observed.

From a detailed analysis of coincidences and intensities of band **E**, especially in connection with the 1297 keV γ-ray transition, band **G** was revealed. Eight γ-ray transitions were obtained for this band up to excitation energy of 14.8 MeV and a spin of $(\frac{51}{2}^-)$. Characteristic for this band is a fragmentary decay near the bandhead, with intensity being distributed over a number of transitions.

A sequence of five γ-ray transitions and tentatively a 2341 keV transition on top of the band were identified for band **H**. This band deexcites via two transitions of 1425 and 1305 keV into band **F** and a strong mixing between both $(\frac{29}{2}^-)$ levels of the two bands was observed. In addition a 1494 keV transition was observed to populate the $(\frac{33}{2}^-)$ state of band **H** and two more γ rays with 1479 and 1553 keV were found to be in coincidence with this transition. Possibly, this sequence of γ rays belongs to another band which is feeding into band **H**.

The cascade of γ lines in band **J** resulted from an investigation of the decay properties of band **G** in connection with the weak low energy γ rays of 379, 444, and 495 keV. Seven new γ transitions were finally assigned to band **J** up to an

excitation energy of 6.9 MeV and a probable spin of $(\frac{33}{2}^-)$.

Band **X** is less intense in the data compared to the other bands and any transitions involved in the decay out of this band were not identified. Therefore level energies and spins for this band are unknown. From the coincidence analysis, this band was found to populate the $\frac{25}{2}^+$ and $\frac{29}{2}^+$ levels of the $(+,+\frac{1}{2})$ yrast band **A**. This indicates a relative position for band **X** above the $\frac{29}{2}^+$ state of band **A**.

In addition to the regular bands several transitions were observed, connecting the proposed negative-parity sequences with the positive-parity states. These transitions and their similarity to transitions observed in the neighboring nuclei ^{79}Rb and ^{83}Y support the proposed spins of the involved levels.

V. INTERPRETATION

A. Configurations at low excitation energy

Nuclei in the mass $A\approx 80$ region are predicted to exhibit a rich variety of features which strongly depend on the number of involved protons and neutrons. In a microscopic view their behavior is primarily determined by the $2p_{3/2}$, $1f_{5/2}$, $2p_{1/2}$, and $1g_{9/2}$ orbitals. The odd proton in ^{81}Y is expected to have a stabilizing influence on the even-even prolate-deformed core ^{80}Sr. Experimentally Lister *et al.* [11] and Mitarai *et al.* [12] have assigned the $[422]\frac{5}{2}^+$ configuration to the ground state, via beta-decay measurements. The occupation of the $[422]\frac{5}{2}^+$ orbital is expected to induce a prolate shape with a quadrupole deformation of $\beta_2 \geqslant 0.3$ [1]. This value agrees with $\beta_2 = 0.39(3)$ and $\beta_2 = 0.33(5)$ for the $\frac{13}{2}^+$ and $\frac{17}{2}^+$ levels, respectively, deduced from their measured lifetimes by Johnson *et al.* [13].

In addition to the $\pi[422]\frac{5}{2}^+$ orbital at prolate deformation, assigned to the positive-parity yrast bands **A** and **B**, possible negative-parity orbitals close to the Fermi surface originate from the $2p_{3/2}$, $1f_{5/2}$, and $2p_{1/2}$ subshells. A possible interpretation for the negative-parity yrast bands **E** and **F** would be a $\pi[301]\frac{3}{2}^-$ configuration. The other two low-lying negative-parity bands, **I** and **J**, are likely built on the $\pi[301]\frac{1}{2}^-$ and the $\pi[303]\frac{5}{2}^-$ orbitals, respectively.

B. Shape evolution

The equilibrium deformation expected in the yttrium nuclei is characterized by an interplay between the spherical $Z,N=40$ gaps and the deformed gaps at $Z,N=38$, 40, 42, and 44 (see Fig. 1 of Ref. [1]) favoring a prolate deformation. These shell-structure effects do strongly influence the nuclear shape dependent on the particle number and the spin.

To study shape transition effects the Woods-Saxon cranking code of Nazarewicz *et al.* [1] was used to calculate total Routhian surfaces (TRS's) for ^{81}Y. In the TRS predictions both signatures and parities were found to behave similarly with increasing rotational frequency. A selection of TRS plots for the $(+,+\frac{1}{2})$ configuration in the (β_2,γ) plane is illustrated in Fig. 9. At low rotational frequencies ($\hbar\omega \leqslant 0.4$ MeV) the TRS predicts a minimum corresponding to a deformed prolate shape ($\beta_2=0.36$, $\gamma\approx 0°$) of the nucleus. With increasing rotational frequency the first alignment of a pair of $g_{9/2}$ particles is expected to trigger a polarization towards a triaxial deformed shape ($\beta_2\approx 0.2$, $\gamma\approx -30°$). This triaxial minimum continues to exist up to high rotational frequencies in coexistence with a noncollective oblate minimum ($\beta_2\approx 0.2$, $\gamma\approx 60°$) and a highly deformed prolate minimum ($\beta_2\approx 0.47$, $\gamma\approx 0°$), which develops above a rotational frequency of 1 MeV. Due to the multiple occurrence of minima in the TRS at high frequencies and their rapid changes as a function of frequency a very complex system of band structures can be expected.

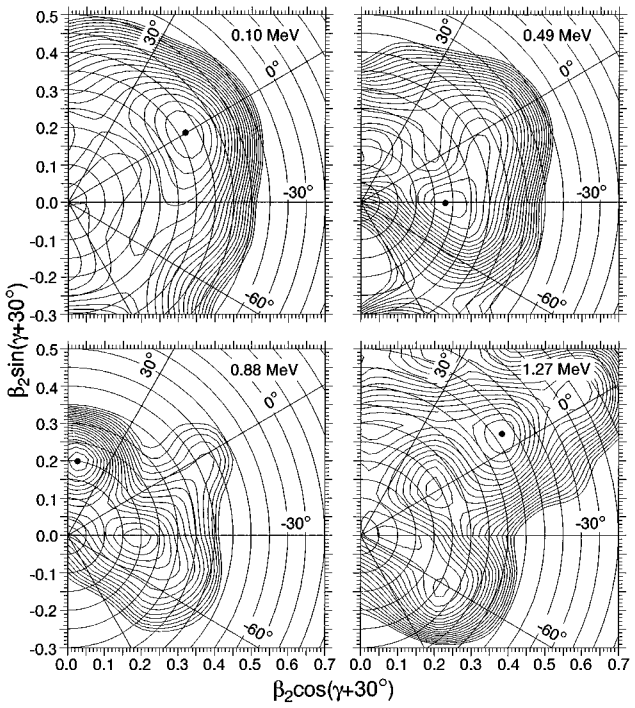

FIG. 9. Total Routhian surfaces in the (β_2,γ) plane for the $(+,+\frac{1}{2})$ configuration in ^{81}Y at different rotational frequencies.

C. Cranked shell-model analysis

In the current investigation of the nucleus ^{81}Y, multiple rotational bands have been observed (Figs. 5 and 6), indicating an appreciable collective behavior of this nucleus up to high spins ($I\approx\frac{55}{2}$). The variety of bands results from an increasing number of possible quasiparticle configurations with spin and makes it difficult to approach the data in a consistent theoretical way. Therefore we will concentrate our discussion on those bands where comparable high-spin data in the odd-A neighboring nuclei is available, the isotone ^{79}Rb [18,19] and the isotope ^{83}Y [17,20].

1. Positive-parity bands

In Fig. 10 the kinematic ($J^{(1)}$) and dynamic ($J^{(2)}$) moments of inertia of four positive-parity bands are compared with the positive-parity states in ^{79}Rb and ^{83}Y. In the nucleus ^{79}Rb a band crossing is observed at $\hbar\omega\approx 0.6$ MeV of the $\pi g_{9/2}$ band, which is interpreted as an alignment of a neutron $g_{9/2}$ pair [21]. A similar feature is observed in the nucleus ^{83}Y. Here the neutron alignment occurs at

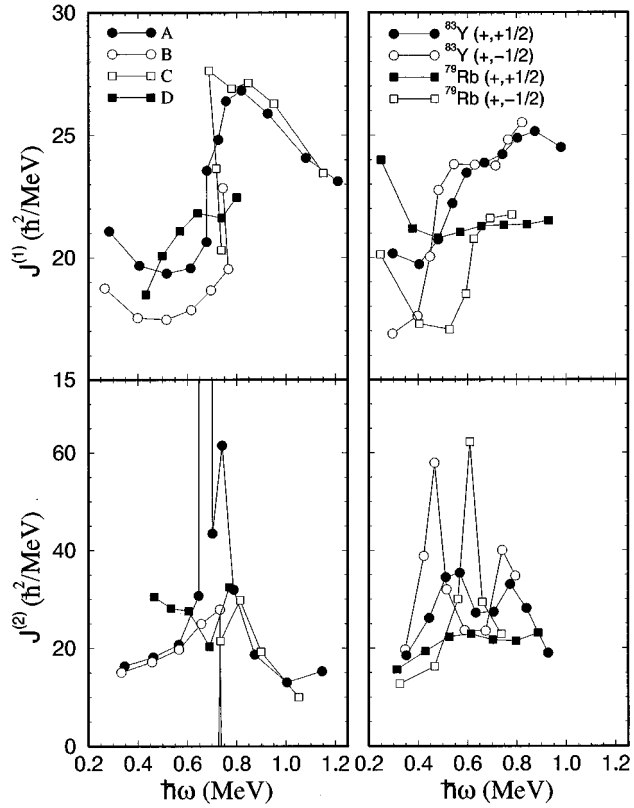

FIG. 10. Observed moments of inertia, $J^{(1)}$ and $J^{(2)}$, as a function of rotational frequency for the positive-parity bands in ^{81}Y compared to positive-parity bands in ^{83}Y and ^{79}Rb.

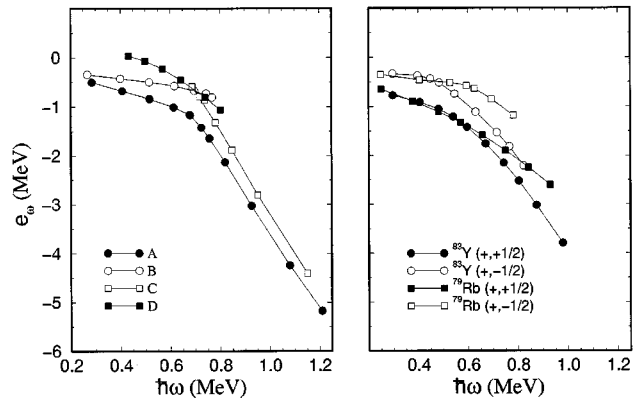

FIG. 11. Experimental Routhian as function of rotational frequency for the positive-parity bands in ^{81}Y compared to positive-parity bands in ^{83}Y and ^{79}Rb. Reference parameters: $J_0 = 16\hbar^2/\mathrm{MeV}$, $J_1 = 1\hbar^4/\mathrm{MeV}^3$.

$\hbar\omega \approx 0.45$ MeV and is followed by a second crossing at $\hbar\omega \approx 0.75$ MeV, which is proposed as the break up of a proton $g_{9/2}$ pair [17].

A careful examination of Fig. 10, regarding the favored signature (band **A**) of the positive-parity yrast band in ^{81}Y shows two upbends in the dynamic moment of inertia $J^{(2)}$ at $\hbar\omega = 0.67$ and 0.74 MeV. The first crossing occurs at a higher frequency when compared to the crossing in ^{83}Y and ^{79}Rb and has been interpreted previously as the alignment of a neutron $g_{9/2}$ pair. The second crossing at $\hbar\omega = 0.74$ MeV is less pronounced in the plot of $J^{(1)}$, but well visible in the $J^{(2)}$ plot. This crossing has not been observed previously and represents probably the break-up of a pair of $g_{9/2}$ protons, as seen in the neighboring nucleus ^{83}Y at $\hbar\omega \approx 0.75$ MeV.

The unfavored signature (band **B**) of the yrast band was observed up to a rotational frequency of $\hbar\omega \approx 0.74$ MeV, where a sharp upbend in $J^{(1)}$ occurs. At this point band **B** is crossed by the new band **C**, which becomes energetically favored as seen in a plot of the experimental Routhians (Fig. 11). For this purpose a common reference had to be subtracted from the experimental level energies. Due to the pronounced shape effects in the $A \approx 80$ nuclei it is difficult to choose a reasonable set of reference parameters for the Harris formula. Thus the parameters $J_0 = 16\hbar^2/\mathrm{MeV}$ and $J_1 = 1\hbar^4/\mathrm{MeV}^3$ reflect a compromise which allows to present the data for the bands discussed in the same graph. Those parameters have also been used earlier in the analysis of ^{79}Rb by Skeppstedt *et al.* [18] and for consistency the same values were chosen for all the nuclei presented in the figure. As seen in Fig. 11, the magnitude of the signature splitting between band **A** and **B** is found to increase up to $\Delta e_\omega \approx 0.6$ MeV at the frequency of the first crossing ($\hbar\omega \approx 0.7$ MeV). After the crossing the separation between the levels in band **A** and **C** remains constant ($\Delta e_\omega \approx 0.4$ MeV) up to a very high rotational frequency of 1.2 MeV. A similar behavior with respect to the signature splitting is observed for the positive-parity bands in ^{79}Rb and ^{83}Y.

The first crossing has been observed in many neighboring odd-A nuclei [17,21–27] and has been interpreted as the alignment of a pair of protons (odd-N nuclei) or neutrons (odd-Z nuclei) in the $g_{9/2}$ orbital, which simultaneously triggers a change in deformation. In the case of ^{81}Y the alignment of a $g_{9/2}$ neutron pair polarizes the nucleus to a shape with negative γ deformation. Theoretically the aligned neutron pair in an $N = 42$ nucleus is predicted to drive the nucleus to a triaxial shape with $\gamma \approx -50°$ (see Fig. 1b in [21]). At this γ deformation a pair of $g_{9/2}$ neutrons is calculated to have the lowest excitation energy. The tendency to negative γ deformation competes with the preference of the odd proton and the core to a more prolate shape. Therefore the equilibrium γ deformation is expected to lie somewhere between $\gamma \approx -50°$ and $\gamma \approx 0°$. From TRS calculations a value of $\gamma = -30°$ is predicted (see Sec. V B and Fig. 9). In this respect, bands **A** and **C** are expected to have a triaxial $\pi g_{9/2} \nu g_{9/2}^2$ configuration above the first neutron crossing frequency. Furthermore band **B** is no longer observed with increasing rotational frequency and band **C** continues to play the role of band **B** as the signature partner of band **A**.

The small increment in $J^{(1)}$ of band **C** at $\hbar\omega = 0.81$ MeV reflects possibly the break-up of the proton $g_{9/2}$ pair, as already seen as a second crossing in band **A** at $\hbar\omega = 0.74$ MeV. The first and second crossing in the unfavored signature are found to occur ≈ 0.07 MeV after the corresponding crossing has taken place in band **A**. Above the frequency of the second crossing the bands **A** and **C** are based on a five-quasiparticle configuration, involving aligned $\nu g_{9/2}^2$ and $\pi g_{9/2}^2$ pairs. For this configuration the moment of inertia $J^{(1)}$ values of the bands **A** and **C** are found to be similar above a frequency of $\hbar\omega \approx 0.9$ MeV. At these high frequencies the Coriolis force reduces the influence of pairing correlations and the moment of inertia of a rotating

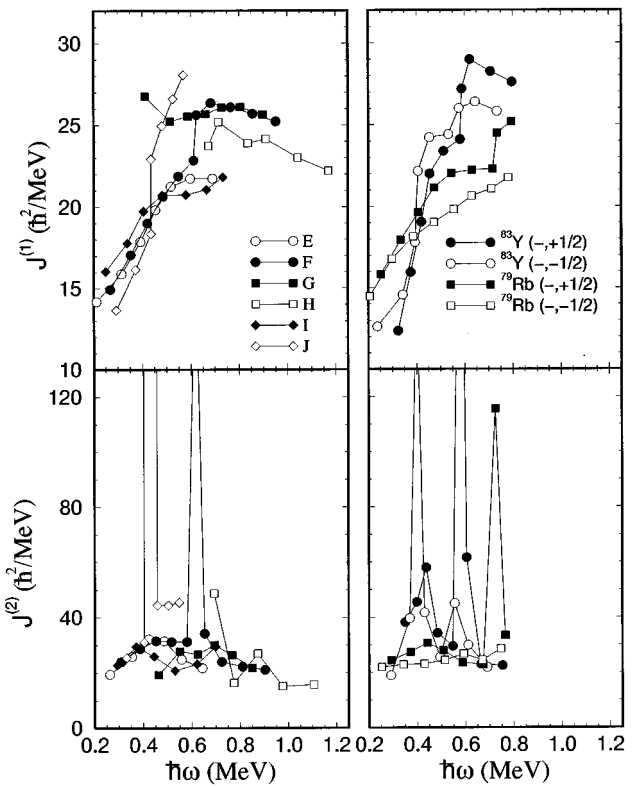

FIG. 12. Observed moments of inertia, $J^{(1)}$ and $J^{(2)}$, as a function of rotational frequency for the negative-parity bands in ^{81}Y compared to negative-parity bands in ^{83}Y and ^{79}Rb.

nucleus is expected to approach the rigid rotor value $J_{\rm rig}(^{81}{\rm Y},\beta_2=0.2)\approx 23\hbar^2/{\rm MeV}$.

In contrast to the rather sharp upbends observed in the $J^{(1)}$ plots for the bands **A**, **B**, and **C**, the rotational band **D** only shows a smoothly rising curve around the rotational frequency of the neutron crossing. No further conclusions could be drawn for this band, because too few transitions have been observed.

Band **X** is not included in the plots of Fig. 10 and Fig. 11. For this band no connection to the lower part of the level scheme has been established, hence the bandhead spin and energy are unknown. The dynamic moments of inertia calculated from the transition energies are almost constant $J^{(2)}\approx 22\hbar^2/{\rm MeV}$ and did not reveal any more characteristic features.

2. Negative-parity bands

The negative-parity bands are based on the excitation of the odd proton from the positive-parity $1g_{9/2}$ subshell into the $2p_{3/2}$, $1f_{5/2}$, or $2p_{1/2}$ negative-parity subshells (see Sec. V A). Therefore the $[422]\frac{5}{2}^+$ proton orbital is no longer occupied and the first crossing in the negative-parity bands is expected to be the alignment of a $g_{9/2}$ proton pair assuming prolate deformation.

Figure 12 shows a representation of the kinematic ($J^{(1)}$) and dynamic ($J^{(2)}$) moments of inertia of the negative-parity bands with comparable bands in ^{79}Rb and ^{83}Y. For all the bands a successive increase in the $J^{(1)}$ moment of inertia at low rotational frequencies is observed. In the case of ^{79}Rb this behavior has been interpreted as the gradual alignment of a $g_{9/2}$ proton pair with large 1qp-3qp band interaction [18]. There, the smooth alignment continues up to a frequency of $\hbar\omega=0.73$ MeV, when a sharp upbend occurs in the favored signature of the negative-parity band, which has been explained as the alignment of a $g_{9/2}$ neutron pair.

In ^{81}Y the bands **E** and **F**, which are comparable to the negative-parity bands in ^{79}Rb, respond in an analogous way to the increasing rotational frequency. The smooth rise in $J^{(1)}$ at low frequencies reflects a broad maximum in the $J^{(2)}$ plot, so that an average frequency of $\hbar\omega\approx 0.45$ MeV could be deduced for the gradual alignment of the $g_{9/2}$ proton pair. After the slow increase in $J^{(1)}$ a sharp rise is observed in the favored signature band **F** at a frequency of $\hbar\omega=0.62$ MeV, whereas the unfavored signature seems to converge to the rigid-body value. This second crossing, which has not been observed in the earlier measurements of this nucleus, enhances the resemblance to the $(-,\pm\frac{1}{2})$ bands in ^{79}Rb and indicates an equivalent alignment scenario for these bands. A gradual alignment of a $g_{9/2}$ proton pair appears at low frequencies, which is followed by a sharp alignment of a $g_{9/2}$ neutron pair at higher frequencies. Note the strong dependence of the alignment pattern with respect to the signature. So far, the second crossing is only observed in the favored signature of the negative-parity bands in both nuclei.

The moment of inertia value of band **I** also develops with a gradual increase at low frequencies and shows an indication of a second upbend at higher frequencies. From the $J^{(2)}$ plot rotational frequencies of $\hbar\omega\approx 0.37$ and 0.7 MeV could be assigned to the proposed proton and neutron alignments, respectively.

Close to the frequency of the proton alignment at 0.43 MeV, a sharp rise is observed in the $J^{(1)}$ and $J^{(2)}$ values of band **J** in contrast to the gradual increase in the other bands. A similar upbend has also been reported in the signature partners of the negative-parity band in ^{83}Y at a frequency of 0.39 and 0.43 MeV. In both nuclei, ^{81}Y and ^{83}Y, this upbend is due to the alignment of a $g_{9/2}$ proton pair. Here, a weak 1qp-3qp band interaction is observed, compared to the alignment pattern in bands **E** and **F**.

The last two bands **G** and **H** evolve at high excitation energies of 3.4 MeV and 5.7 MeV, respectively. Band **G** responds in a distinctly different way to the increasing rotational frequency, when compared to the rotational bands of both parities discussed so far. This band shows a rather constant moment of inertia of $J^{(1)}\approx 26\hbar^2/{\rm MeV}$ over a large frequency range of $\hbar\omega=0.5-1.0$ MeV. The relatively high value of $J^{(1)}$ suggests a rigid rotor motion. Assuming a prolate shape for the nucleus, this value corresponds to a large deformation of $\beta_2=0.44$. Probably this band belongs to the highly deformed minimum at $\beta_2=0.47$, in the TRS calculations (see Sec. V B).

An observation which deserves comments is that the moment of inertia is comparable to values typical for superdeformed bands in the mass $A\approx 80$ region, but excitation energy $E_x=3.4$ MeV and spin $I=(\frac{19}{2})$ of this band are surprisingly low to the usually observed values for suggested superdeformed bands in this mass region, e.g., ^{83}Sr,

$E_x \approx 13$ MeV, $I \approx (\frac{41}{2})$ [7]. Interestingly, the tendency of superdeformed bands to have a fragmentary decay near their bandheads, with intensity being distributed over a number of transitions (e.g., Fig. 2 in [7]), is observed for band **G**, too. It would be interesting to further investigate the nature of this phenomenon and to establish a lifetime analysis of the band members for a systematic comparison with quadrupole moments deduced for superdeformed bands in nuclei with $A \approx 80$.

Band **H** starts above a high rotational frequency of 0.6 MeV (above the neutron alignment) and shows a decreasing moment of inertia with increasing frequency, approaching the rigid rotor value as observed in the positive-parity states. At $\hbar\omega = 0.87$ MeV a fluctuation in the dynamic moment of inertia is observed, indicating an interaction with an intruder orbital. Too few states have been observed for this band in order to deduce any further conclusions.

3. Band termination

In a nucleus with a small number of particles outside closed shells the total angular momentum available from the spin alignment of the particles (and holes) is limited. A particular configuration giving rise to a collective band is expected to gradually lose collectivity with increasing spin and eventually terminate [28]. Such terminating bands are well known in several $A \sim 110$ nuclei (e.g., [29–31]) and are also expected in other mass regions. Recently, evidences for such bands in the $A \sim 80$ region have been reported in the nuclei ^{74}Kr and ^{82}Sr [32,33].

In ^{81}Y the bands **A**, **C**, **G**, **F**, and **H** have been extended to considerable high-spin values of $I \approx \frac{55}{2}$, a spin region where possible termination effects are expected to evolve for bands with a few particles in the $g_{9/2}$ subshell. A characteristic feature of terminating bands is a gradual decrease in the moment of inertia with increasing rotational frequency, a reflection of the fact that the angular momentum is predominantly built by the aligning particles. This decrease in the moment of inertia is observed for the bands **A**, **C**, and **H** above $\hbar\omega = 0.9$ MeV (see Figs. 10 and 12). A further indication of band termination is the high energy cost, necessary for building the last spin values. This unfavored energy consumption manifests itself as a characteristic ''parabola''-like curve when the excitation energy versus spin is plotted relative to a rigid rotor reference. This has been done in Fig. 13 for the bands **A**, **C**, and **H**, relative to a rigid rotor with a moment of inertia of 23 $\hbar^2$/MeV. For these bands an upbend is seen above a spin of $I \approx 24$, indicating that the spin of the highest levels within the bands are approaching termination. Possibly those structures are based on the four unpaired protons and neutrons in the $g_{9/2}$ subshell coupling to the above spin value in the terminating state.

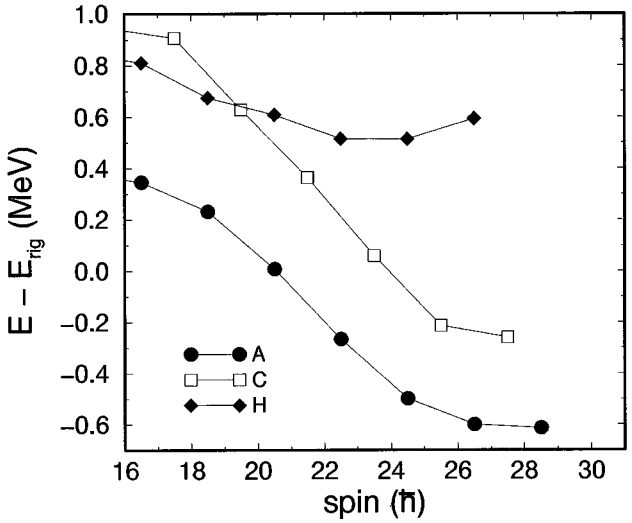

FIG. 13. Experimental $E - E_{\rm rig}$ curves for the bands **A**, **C**, and **H** as function of spin. The energies are given relative to a rigid rotor reference $E_{\rm rig} = (\hbar^2/2J_{\rm rig})I(I+1)$, with a moment of inertia $J_{\rm rig} = 23\hbar^2$/MeV.

VI. CONCLUSIONS

In the present investigation the high-spin structure of the nucleus ^{81}Y has been studied. The combination of the GAMMASPHERE array for γ-ray detection and the simultaneous identification of emitted charged particles by the MICROBALL detector proved to be an essential tool for a detailed spectroscopy of this nucleus. Despite the small number of counts which have been collected for this nucleus during the experiment, clean spectra have been achieved by selecting the desired reaction channel with the charged-particle detector. Furthermore, from an event-by-event determination of the nucleus recoil momentum a precise Doppler-shift correction has been applied to the γ rays, leading to resolution-enhanced γ lines in the spectra.

The analysis of an E_γ-E_γ matrix as well as an E_γ-E_γ-E_γ cube resulted in the placement of more than 100 new γ rays and 80 new levels in the decay scheme of ^{81}Y. Most of the new levels have been assigned to rotational bands, where six bands have been observed. Several bands have been extended up to an excitation energy of 17 MeV with the top spin reaching $I = (\frac{57}{2})$.

Levels at low excitation energy have been interpreted systematically by configurations built on the proton single-particle levels $[422]\frac{5}{2}^+$, $[301]\frac{3}{2}^-$, $[303]\frac{5}{2}^-$, and $[301]\frac{1}{2}^-$. Possible evidence for a $[301]\frac{1}{2}^-$ level close to the ground state has been found time in this nucleus.

In the favored signature of the positive-parity yrast band a second band crossing has been observed. These crossings have been interpreted similarly to characteristic crossings observed in the neighboring nuclei ^{79}Rb and ^{83}Y. On the basis of systematics the first is attributed to $g_{9/2}$ neutrons and the second to $g_{9/2}$ protons. With increasing rotational frequency a convergence of the moments of inertia close to the rigid body value has been found.

Regarding the negative-parity bands the successive increase in the $J^{(1)}$ moment of inertia at low rotational frequency has been interpreted as the gradual alignment of a proton $g_{9/2}$ pair. At higher frequencies a breakup of a $g_{9/2}$ neutron pair has been observed only in the favored signature of the negative-parity yrast band. An equivalent alignment scenario has been reported in the neighboring isotone ^{79}Rb.

A band associated with a high moment of inertia has been

found ($J^{(1)} \approx 26\hbar^2/\mathrm{MeV}$). The value remains constant over a large frequency range and lies close to the moments of inertia deduced for superdeformed bands in the $A \approx 80$ nuclei. This band has been observed at strikingly lower spin and excitation energy as compared to the superdeformed bands known so far. Further investigations, including the measurement of the quadrupole moment are necessary in order to classify this band as being associated with a highly deformed nuclear shape.

Three bands have been extended to considerable high spin values of $I \approx \frac{55}{2}$ and have been found to exhibit the characteristic features of terminating bands.

ACKNOWLEDGMENTS

This work was supported in part by the Bundesministerium für Bildung, Wissenschaft, Forschung und Technologie (BMBF) under Contract No. 06DR666I, the U.S. National Science Foundation under Grant No. PHY-9210082 (FSU), and the U.S. Department of Energy, under Contract Nos. DE-AC03-76SF00098 (LBNL), DE-FG05-88ER40406 (Washington University), DE-AC05-76OR00033 (UNISOR), and DE-AC05-960R22464 (ORNL) with Lockheed Martin Energy Research Corporation. We also wish to thank the staff of the LBNL (GAMMASPHERE) facility.

[1] W. Nazarewicz, J. Dudek, R. Bengtsson, T. Bengtsson, and I. Ragnarsson, Nucl. Phys. **A435**, 397 (1985).

[2] J. Dudek, W. Nazarewicz, and N. Rowley, Phys. Rev. C **35**, 1489 (1987).

[3] C. J. Lister, B. J. Varley, H. G. Price, and J. W. Olness, Phys. Rev. Lett. **49**, 308 (1982).

[4] C. Baktash, G. Garcia-Bermudez, D. G. Sarantites, W. Nazarewicz, V. Abenante, J. R. Beene, H. C. Griffin, M. L. Halbert, D. C. Hensley, N. R. Johnson, I. Y. Lee, F. K. McGowan, M. A. Riley, D. W. Stracener, T. M. Semkow, and A. Virtanen, Phys. Lett. B **255**, 174 (1991).

[5] C. Baktash, D. M. Cullen, J. D. Garrett, C. J. Gross, N. R. Johnson, W. Nazarewicz, D. G. Sarantites, J. Simpson, and T. R. Werner, Phys. Rev. Lett. **74**, 1946 (1995).

[6] H.-Q. Jin, C. Baktash, M. J. Brinkman, C. J. Gross, D. G. Sarantites, I. Y. Lee, B. Cederwall, F. Cristancho, J. Döring, F. E. Durham, P.-F. Hua, G. D. Johns, M. Korolija, D. R. LaFosse, E. Landulfo, A. O. Macchiavelli, W. Rathbun, J. X. Saladin, D. W. Stracener, S. L. Tabor, and T. R. Werner, Phys. Rev. Lett. **75**, 1471 (1995).

[7] D. R. LaFosse, P.-F. Hua, D. G. Sarantites, C. Baktash, Y. A. Akovali, M. Brinkman, B. Cederwall, F. Cristancho, J. Döring, C. J. Gross, H.-Q. Jin, M. Korolija, E. Landulfo, I. Y. Lee, A. O. Macchiavelli, M. R. Maier, W. Rathbun, J. X. Saladin, D. W. Stracener, S. L. Tabor, A. Vander Mollen, and T. R. Werner, Phys. Lett. B **354**, 34 (1995).

[8] A. G. Smith, P. J. Dagnall, J. C. Lisle, D. H. Smalley, T. R. Werner, R. Chapman, C. Finck, B. Haas, M. Leddy, W. Nazarewicz, D. Prévost, N. Rowley, and H. Savajols, Phys. Lett. B **355**, 32 (1995).

[9] F. Cristancho, D. R. LaFosse, C. Baktash, D. F. Winchell, B. Cederwall, J. Döring, C. J. Gross, P.-F. Hua, H.-Q. Jin, M. Korolija, E. Landulfo, I. Y. Lee, A. O. Macchiavelli, M. R. Maier, W. Rathbun, J. X. Saladin, D. Sarantites, D. W. Stracener, S. L. Tabor, A. Vander Mollen, and T. R. Werner, Phys. Lett. B **357**, 281 (1995).

[10] P. J. Dagnall, A. G. Smith, J. C. Lisle, D. H. Smalley, R. Chapman, C. Finck, B. Haas, M. Leddy, D. Prévost, N. Rowley, and H. Savajols, Z. Phys. A **353**, 251 (1995).

[11] C. J. Lister, R. Moscrop, B. J. Varley, H. G. Price, E. K. Warburton, J. W. Olness, and J. A. Becker, J. Phys. G **11**, 969 (1985).

[12] S. Mitarai, T. Kuroyanagi, A. Odahara, J. Mukai, H. Tomura, S. Suematsu, T. Morikawa, D. Jerrestam, J. Nyberg, G. Sletten, A. Atac, M. Piiparinen, S. E. Arnell, D. Foltescu, H. A. Roth, and Ö. Skeppstedt, Nucl. Phys. **A557**, 381c (1993).

[13] T. D. Johnson, A. Raguse, C. J. Gross, M. K. Kabadiyski, K. P. Lieb, D. Rudolph, M. Weiszflog, T. Burkardt, J. Eberth, and S. Skoda, Z. Phys. A **350**, 189 (1994).

[14] Gammasphere Report LBL-PUB-**5202**; I. Y. Lee, Nucl. Phys. **A520**, 641c (1990).

[15] D. G. Sarantites, P.-F. Hua, M. Devlin, L. G. Sobotka, J. Elson, J. T. Hood, D. R. LaFosse, J. E. Sarantites, and M. R. Maier, Nucl. Instrum. Methods Phys. Res. A **381**, 418 (1996).

[16] D. C. Radford, Nucl. Instrum. Methods Phys. Res. A **361**, 297 (1995).

[17] F. Cristancho, C. J. Gross, K. P. Lieb, D. Rudolph, Ö. Skeppstedt, M. A. Bentley, W. Gelletly, H. G. Price, J. Simpson, J. L. Durell, B. J. Varley, and S. Rastikerdar, Nucl. Phys. **A540**, 307 (1992).

[18] Ö. Skeppstedt, C. J. Lister, A. A. Chishti, B. J. Varley, W. Gelletly, U. Lenz, R. Moscrop, and L. Goettig, Nucl. Phys. **A511**, 137 (1990).

[19] J. W. Holcomb, J. Döring, T. Glasmacher, G. D. Johns, T. D. Johnson, M. A. Riley, P. C. Womble, and S. L. Tabor, Phys. Rev. C **48**, 1020 (1993).

[20] C. J. Lister, B. J. Varley, W. Fieber, J. Heese, K. P. Lieb, E. K. Warburton, and J. W. Olness, Z. Phys. A **329**, 413 (1988).

[21] R. Bengtsson, W. Nazarewicz, Ö. Skeppstedt, and R. Wyss, Nucl. Phys. **A528**, 215 (1991).

[22] L. Funke, J. Döring, P. Kemnitz, E. Will, G. Winter, A. Johnson, L. Hildingsson, and Th. Lindblad, Nucl. Phys. **A455**, 206 (1986).

[23] P. Kemnitz, J. Döring, L. Funke, G. Winter, L. H. Hildingsson, D. Jerrestam, A. Johnson, and Th. Lindblad, Nucl. Phys. **A456**, 89 (1986).

[24] E. F. Moore, P. D. Cottle, C. J. Gross, D. M. Headly, U. J. Hüttmeier, S. L. Tabor, and W. Nazarewicz, Phys. Rev. C **38**, 696 (1988).

[25] G. Winter, J. Döring, L. Funke, H. Prade, H. Rotter, R. Schwengner, A. Johnson, and A. Nilsson, J. Phys. G **14**, L13 (1988).

[26] S. L. Tabor, P. D. Cottle, C. J. Gross, U. J. Hüttmeier, E. F. Moore, and W. Nazarewicz, Phys. Rev. C **39**, 1359 (1989).

[27] R. Schwengner, J. Döring, L. Funke, G. Winter, A. Johnson, and W. Nazarewicz, Nucl. Phys. **A509**, 550 (1990).

[28] A. V. Afanasjev and I. Ragnarsson, Nucl. Phys. **A591**, 387 (1995).

[29] V. P. Janzen, D. R. LaFosse, H. Schnare, D. B. Fossan, A. Galindo-Uribarri, J. R. Hughes, S. M. Mullins, E. S. Paul, L. Persson, S. Pilotte, D. C. Radford, I. Ragnarsson, P. Vaska, J. C. Waddington, R. Wadsworth, D. Ward, J. Wilson, and R. Wyss, Phys. Rev. Lett. **72**, 1160 (1994).

[30] R. Wadsworth, C. W. Beausang, M. Cromaz, J. DeGraaf, T. E. Drake, D. B. Fossan, S. Flibotte, A. Galindo-Uribarri, K. Hauschild, I. M. Hibbert, G. Hackman, J. R. Hughes, V. P. Janzen, D. R. LaFosse, S. M. Mullins, E. S. Paul, D. C. Radford, H. Schnare, P. Vaska, D. Ward, J. N. Wilson, and I. Ragnarsson, Phys. Rev. C **53**, 2763 (1996).

[31] H. Schnare, D. R. LaFosse, D. B. Fossan, J. R. Hughes, P. Vaska, K. Hauschild, I. M. Hibbert, R. Wadsworth, V. P. Janzen, D. C. Radford, S. M. Mullins, C. W. Beausang, E. S. Paul, J. DeGraaf, I. Y. Lee, A. O. Macchiavelli, A. V. Afanasjev, and I. Ragnarsson, Phys. Rev. C **54**, 1598 (1996).

[32] D. Rudolph (private communication).

[33] D. M. Cullen (private communication).